Journal of chemical & engineering data

Article

pubs.acs.org/jced

Experimental and Modeling Study of the Phase Behavior of (Heptane + Carbon Dioxide + Water) Mixtures

Saif. Z. S. Al Ghafri,[†] Esther Forte,[‡,§] Amparo Galindo,[†,‡] Geoffrey C. Maitland,[†] and J. P. Martin Trusler*[,†]

[†]Qatar Carbonates and Carbon Storage Research Centre, and [‡]Centre for Process Systems Engineering, Department of Chemical Engineering, Imperial College London, South Kensington Campus, London SW7 2AZ, U. K.

ABSTRACT: We report experimental measurements of three-phase equilibria in the system (heptane + carbon dioxide + water) obtained with a quasi-static analytical apparatus with compositional analysis by means of gas chromatography. The apparatus was calibrated by an absolute area method and the whole measurement system was validated by means of comparison with the published literature data of the system (heptane + carbon dioxide). The compositions of the three phases coexisting in equilibrium were measured along five isotherms at temperatures from (323.15 to 413.15) K with pressures ranging from approximately 2 MPa to the upper critical end point pressure at which the two nonaqueous phases became critical. The experimental results have been compared with the predictions of the statistical associating fluid theory for potentials of variable range. The unlike binary interaction parameters used here are consistent with a previous study for a ternary mixture of a different *n*-alkane, while the alkane−water binary interaction parameter is found to be transferable and the alkane−carbon dioxide binary interaction parameter is predicted using a modified Hudson-McCoubrey combining rule. Generally, good agreement between experiment and theory was found.

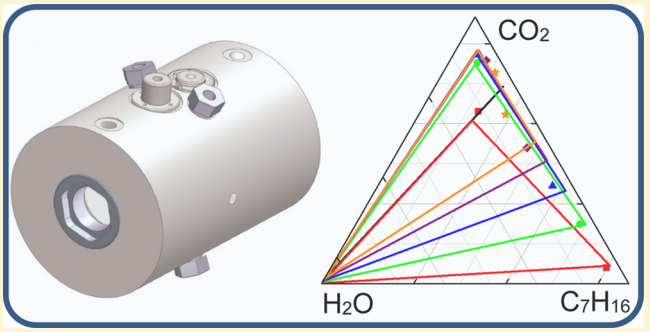

1. INTRODUCTION

Knowledge of the phase behavior of mixtures containing hydrocarbons, CO_2 and H_2O plays an essential role in the design and operation of effective and economical processes involving reservoir fluids and CO_2. However, due to the vast number of components that they may contain and the lack of a detailed characterization, treatment of such mixtures is challenging both experimentally and theoretically. Hence to gain a better understanding of the phase behavior of mixtures of oil with CO_2 and H_2O, studies of simpler model systems that represent certain characteristics of the real ones may provide a platform for dealing with systems containing more complex hydrocarbon mixtures. Despite their importance as a simpler representation of reservoir fluids, experimental data for (hydrocarbon + CO_2 + H_2O) mixtures are scarce and limited to vapor−liquid equilibrium (VLE) measurements in most of the cases.

Table 1 summarizes the published data for systems of the type (*n*-alkane + CO_2 + H_2O). The mixture (CH_4 + CO_2 + H_2O) is the most widely studied system in this class, with both VLE[1−4] and fluid-hydrate equilibria[5−10] reported. However, only in the recent work of Al Ghafri et al.[11] was the three-phase vapor−liquid−liquid (VLLE) region also studied. In that work, the system (CH_4 + CO_2 + water) was studied in the regions of two-phase VLE, three-phase VLLE, and four-phase vapor−liquid−liquid−hydrate equilibrium at temperatures from (285 to 423) K and pressures from (2 to 20) MPa. Forte et al.[12] studied VLLE for ($C_{10}H_{22}$ + CO_2 + H_2O) at temperatures from (323 to 413) K and pressures from (1 to 18) MPa. The same authors[13] also studied VLLE of (C_3H_8 + CO_2 + H_2O) at temperatures from (311 to 353) K and pressures from (1.7 to 6.7) MPa. In each of these studies, the VLLE data were compared with the predictions of the statistical associating fluid theory for potentials of variable range (SAFT-VR).[14,15] The only other relevant study is that of Brunner et al.,[16] who studied VLLE for ($C_{16}H_{34}$ + CO_2 + H_2O) at temperatures of (473.15 and 573.15) K and pressures of (20.1 and 30.1) MPa.

The current paper on (C_7H_{16} + CO_2 + H_2O) is a continuation of our previous experimental and modeling studies of other (*n*-alkane + CO_2 + H_2O) mixtures.[11−13]

To model this system, an approach able to capture the nature of the molecules and their interactions is highly desirable. In this work we use the SAFT-VR equation of state,[14,15] which is a version of the Statistical Associating Fluid Theory (SAFT).[17,18] SAFT stems from the first order perturbation theory of Wertheim,[19−22] and accounts for the possibility of chain formation and directional interactions. These features of the theory are especially relevant to the nonsphericity of alkanes and the hydrogen-bonding association of water. The

Special Issue: Memorial Issue in Honor of Anthony R. H. Goodwin

Received: July 20, 2015
Accepted: October 16, 2015
Published: November 2, 2015

DOI: 10.1021/acs.jced.5b00618
J. Chem. Eng. Data 2015, 60, 3670−3681

Table 1. Literature Data for Ternary Mixtures of the Type (*n*-Alkane + CO_2 + H_2O)

ref	system	equilibria	T_{min} K	T_{max} K	p_{min} MPa	p_{max} MPa
4	CH_4 + H_2O + CO_2	VLE	324.30	375.50	10.5	50.6
1	CH_4 + H_2O + CO_2	VLE	344.15	344.15	10	100
2	CH_4 + H_2O + CO_2	VLE	298.75	323.15	6.2	13.8
3	CH_4 + H_2O + CO_2	VLE	243.1	288.4	0.11	6.05
11	CH_4 + H_2O + CO_2	VLLE	285.15	303.15	4.93	8.63
3	C_2H_6 + H_2O + CO_2	VLE	252.20	288.4	0.11	2.03
67	C_3H_8 + H_2O + CO_2	VLE	247.50	289.00	0.1	2.1
13	C_3H_8 + H_2O + CO_2	VLLE	311.10	353.18	1.67	6.71
67	C_4H_{10} + H_2O + CO_2	VLE	252.90	288.30	0.1	2.1
12	$C_{10}H_{22}$ + H_2O + CO_2	VLLE	323.08	413.16	0.94	18.12
16	$C_{16}H_{34}$ + H_2O + CO_2	VLLE	473.15	573.15	10.1	30.1

description of aqueous systems with equations of state is not a simple task, especially in mixtures with a nonpolar compound such as an alkane. These systems are characterized by large regions of immiscibility. The alkane in the aqueous phase is highly diluted and polarized inside a hydrogen-bonded network of water molecules, while the environment of water in the alkane-rich phase is completely different. It has been shown that binary interaction parameters can be expressed as a function of both the nature of the interactions between the particular pair of unlike molecules and the characteristics of the medium as a whole.[23] One can therefore anticipate that modeling the extreme nature of these phases with a single binary interaction parameter that describes the unlike interaction between the molecules in all coexisting phases may not provide the best description.

The applicability of associating models to describe the phase behavior of aqueous alkane systems has been a matter of considerable study.[24−37] For mixtures of carbon dioxide with water, cross-association models have been suggested,[38−40] but here we do not make use of these, as SAFT-VR has been shown to be capable of capturing the features of the phase diagram without the need to include cross-association.[41−43] The SAFT-VR formalism has also been shown to be successful in its application to a wide variety of systems. Here we test the application of SAFT-VR to the system (C_7H_{16} + CO_2 + H_2O) and we largely avoid readjustment of parameters from previous work: only the unlike interaction parameter for the (C_7H_{16} + CO_2) system is recalculated based on a modification of the Hudson and McCoubrey combining rules;[23] that for (C_7H_{16} + H_2O) is transferred from a previous study of ($C_{10}H_{22}$ + H_2O).[12]

This paper is organized as follows. In section 2, the experimental apparatus, the methodology, and the materials used are described. In section 3, the theory is described while, in section 4, comparisons between experiment and the model are made. In addition, the influence of adding a third component on the phase behavior of each binary subsystem is analyzed.

2. EXPERIMENTAL SECTION

2.1. Materials. The materials used are detailed in Table 2. The purity of the CO_2 was investigated by gas chromatography

Table 2. Description of Chemical Samples[a]

chemical name	source	purity as supplied[a]	analysis method	additional purification
carbon dioxide	BOC	$x \geq 0.99995$		none
heptane	Sigma-Aldrich	$w \geq 0.995$	GC-FID[b]	none
hexane	Sigma-Aldrich	$w \geq 0.990$		none
tetrahydrofuran	Sigma-Aldrich	$w \geq 0.999$		none
helium	BOC	$x \geq 0.99995$		none
hydrogen	BOC	$x \geq 0.99995$		none
water	Millipore Direct-Q UV3	$\rho_e > 18$ MΩ·cm at $T = 298$ K		degassed under vacuum

[a]Notation: x is mole fraction, w is mass fraction, and ρ_e is electrical resistivity. [a]Purities are as stated by the supplier except where an analysis method is specified. [b]Gas chromatography with flame ionization detector.

(GC) with a thermal conductivity detector (TCD), but no impurities were detected and the purity reported in Table 2 is therefore the minimum mole fraction specified by the supplier. The purity of the C_7H_{16} was investigated by GC with a flame ionization detector (FID), and one impurity, identified from its retention time as hexane, was detected with a mass fraction of 0.5 %. The purity of the H_2O was verified by electrical resistivity measurements.

2.2. Apparatus. The quasi-static analytical apparatus described by Forte et al.[12] was used in the present study. This apparatus, illustrated in Figure 1, comprised a high-pressure equilibrium view cell housed in a thermostatic silicone-oil bath and fitted with a magnetic recirculation pump and gas- and liquid-sampling valves for composition measurements by means of online gas chromatography.

The view cell was a horizontally orientated cylindrical vessel of 35 cm^3 capacity fitted with axially opposed sapphire windows to permit observation of the interior. A two-channel pump was used to recirculate the gas phase and one of the two liquid phases so as to promote equilibration. By tilting the vessel, either the more-dense or the less-dense liquid phase could be recirculated. A four-port chromatographic sampling value with a 1 μL internal loop, inserted in the liquid recirculation path, was used to acquire samples of the liquid phases for analysis. The gas phase was sampled by means of a six-port gas sampling valve connected to the top of the equilibrium cell by a short length of a fine capillary.

Heated transfer tubes connected the liquid- and gas-sampling valves to the inlet of the gas chromatograph (GC) and, during analysis, samples were entirely vaporized after entering these lines. The GC was equipped with a HayeSep Q column (80/100 mesh, 2 m long, 3.2 mm o.d., 2 mm i.d.) and both thermal conductivity (TCD) and flame ionization (FID) detectors. In the present work, the TCD was used to detect water and carbon dioxide, while the FID was used to detect heptane. The instrument conditions used for the GC analyses are detailed in Table 3.

Referring to Figure 1, the refrigerated automatic syringe pump E-3 was used to inject carbon dioxide into the cell

DOI: 10.1021/acs.jced.5b00618
J. Chem. Eng. Data 2015, 60, 3670−3681

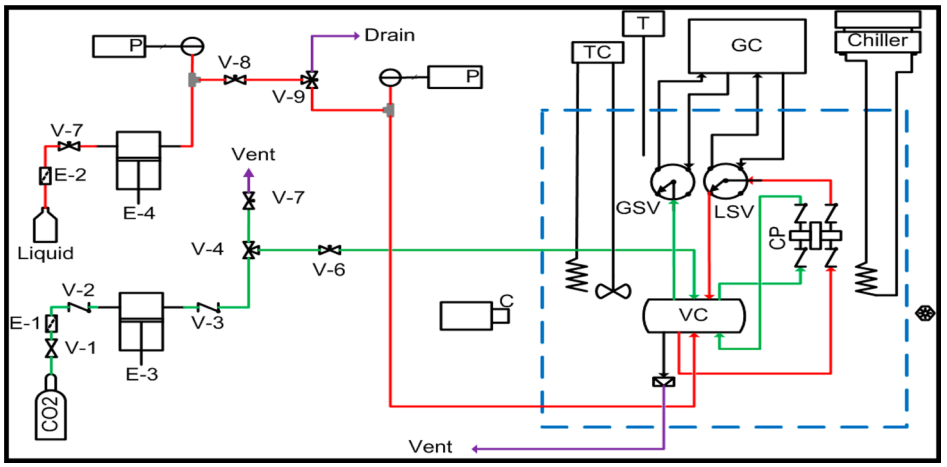

Figure 1. Schematic diagram of the analytical apparatus: E-3 and E-4, correspond to the pumps; GC, VC, CP, TC, GSV, LSV, P, and T, correspond to the gas chromatograph, view cell, reciprocating pump, temperature controller, gas sampling valve, liquid sampling valve, pressure sensor, and temperature sensor, respectively; red and green lines denote the liquid and gas components paths, respectively.

Table 3. Gas Chromatography Conditions for the Analysis of the Mixtures Studied in This Work[a]

injector	column		thermal-conductivity detector		flame-ionization detector	
$\dot{V}$/(cm^3·s^{-1})	T/K	T/K	T/K	I/mA	T/K	φ
40	423.15	343.15	523.15	90	523.15	1:10

[a]Notation: $\dot{V}$ is the carrier-gas flow rate, T is temperature, I is filament current, and φ = H_2/air flow-rate ratio.

through valve V-6, while the manual syringe pump E-4 was used for water and heptane injections through valve V-9. Additionally, valves V-4, V-7, and V-9 were used for venting, rinsing, emptying, and evacuating the cell. The pressure was measured by means of a pressure transducer (Paroscientifc Digiquartz model 410 KR-HT-101) with a full-scale range of 69 MPa located in the liquid inlet line. The temperature was measured with a platinum resistance thermometer positioned in the thermostatic bath close to the cell.

2.3. Calibration. The pressure transducer was calibrated[12] from (0.1 to 50) MPa against a pressure balance having a standard relative uncertainty of 0.005 % and full-scale range of 50 MPa (Desgranges et Huot, model 26000). Following this calibration and periodic adjustment of the zero reading to compensate for drift, the overall standard uncertainty of the pressure is estimated to be 5 kPa. The platinum resistance thermometer was calibrated on ITS-90 in a triple-point of water cell and by comparison in a thermostatic bath with a standard platinum resistance thermometer at temperatures up to 473.15 K. Considering calibration uncertainties, drift and bath-temperature fluctuations, the overall standard uncertainty of temperature was estimated to be 0.05 K.

The two GC detectors were calibrated by an absolute-area method in which samples of the components were injected individually from the fixed volume of the LSV. The amount injected was therefore proportional to the density of the calibration fluid under the conditions at which the LSV was filled. Calibrations were carried out over an extended range so that extrapolation beyond the calibrated range was never required. During calibration, the colum and detectors were operated at the same conditions used for the subsequent analyses.

When calibrating the TCD for CO_2, the amount injected was varied by adjusting the pressure and temperature, and the density was calculated from the equation of state (EoS) of Span and Wagner[44] with an estimated standard relative uncertainty of 0.025 %. Considering repeatability, the standard relative uncertainty in the peak area for CO_2 was estimated to be 1.0 %. Considering uncertainties in temperature, pressure, and the EoS model, the standard relative uncertainty of the density of the CO_2 filling the LSV loop was estimated to be 0.1 %. The relation between peak area and amount of CO_2 injected was found to be slightly nonlinear and a quadratic relationship was therefore used for this component.

When the TCD was calibrated for water, the amount injected was adjusted by diluting the water with varying amounts of tetrahydrofuran. The mixtures were prepared gravimetrically, and the density at the injection conditions was obtained from Schedemann et al.[45] Considering repeatability, the standard relative uncertainty in the peak area for H_2O was estimated to be 2.0 %. Considering uncertainties in temperature, pressure, and the density data, the standard relative uncertainty of the density of the H_2O in the LSV loop was estimated to be 0.2 %. The TCD exhibited a linear response to water.

When calibrating the FID for heptane, the amount injected was adjusted by diluting the heptane with varying amounts of hexane. The mixtures were prepared gravimetrically and the density at the injection conditions was obtained from Ramos-Estrada et al.[46] Considering repeatability, the standard relative uncertainty in the peak area for heptane was estimated to be 1.0 %. Considering uncertainties in temperature, pressure, and the density data, the standard relative uncertainty of the density of the heptane in the LSV loop was estimated to be 0.1 %. The respose of the FID to heptane was linear.

Periodically during, and also after, this work the GC calibrations were checked, and no drift was observed.

2.4. Experimental Procedure. The experimental protocol was essentially as described previously.[12] The apparatus was initially cleaned with solvents, flushed with CO_2 and subjected to vacuum. Then heptane was loaded through valve V-9 until it occupied approximately one-third of the cell volume, after which water was introduced slowly to the cell until the existence of two phases was observed (each occupying approximately one-third of the cell volume). Finally, CO_2 was introduced slowly through valve V-6 until the desired initial

DOI: 10.1021/acs.jced.5b00618
J. Chem. Eng. Data 2015, 60, 3670−3681

pressure was reached at the given temperature. The pressure could then be raised to reach the next state point by injection of further CO_2. While locating the upper critical end point (UCEP) at a given temperature, small adjustments of pressure were carried out by injecting or venting water.

As shown in Figure 2, the UCEP was associated with intense critical opalescence and, ultimately, opacity at the critical point.

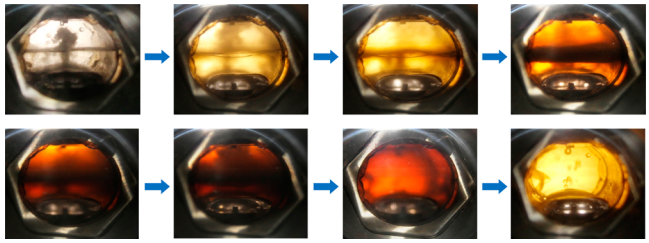

Figure 2. Images of the interior of the vessel showing the critical opalescence phenomena (UCEP) observed between the C_7H_{16}-rich and CO_2-rich gas phases (middle and upper, respectively) at T = 323.15 K. Pressure is raised approximately from (9.01 to 9.08) MPa in moving from the first to the last image.

The composition at the UCEP was estimated by taking samples of the two phases coexisting at a pressure (0.01 to 0.02) MPa above the critical.

2.5. Uncertainty Analysis. The combined standard uncertainty of the mole fraction of each component in a given phase $u(x_i)$ was obtained by Gaussian error propagation according to the relation:

$$u^2(x_i) = \sum_{j=1}^{n}\left[\left(\frac{\partial x_i}{\partial z_j}\right)^2 u^2(z_j)\right] \tag{1}$$

where z_j (j = 1, 2, 3 ⋯ n) are the n independent variables upon which x_i is dependent, each associated with variance $u^2(z_j)$. As in our previous work,[11−13] an absolute area method was used in which the chromatographic peak area A_i associated with substance i is related to the amount n_i of that substance in the sample. For the purposes of this uncertainty analysis, the relationship between n_i and A_i is assumed to be

$$n_i = f_i A_i \tag{2}$$

where f_i is the chromatographic response factor. The mole fraction x_i of component i is therefore given by

$$x_i = A_i f_i / \left(\sum_{k=1}^{N_c} A_k f_k\right) \tag{3}$$

The independent variables to be considered in the uncertainty analysis are temperature, pressure, peak area, and the response factors (obtained by calibration); sample-loop volume is not considered as, if constant, it cancels out exactly in the analysis. Thus, according to eqs 1 and 3,

$$u^2(x_i) = (\partial x_i/\partial T)^2 u^2(T) + (\partial x_i/\partial p)^2 u^2(p) + \sum_{j=1}^{N_c}\left(\frac{\partial x_i}{\partial n_j}\frac{\partial n_j}{\partial A_j}\right)^2 u^2(A_j) + \sum_{j=1}^{N_c}\left(\frac{\partial x_i}{\partial n_j}\frac{\partial n_j}{\partial f_j}\right)^2 u^2(f_j) \tag{4}$$

where N_c is the number of components. Since the partial derivatives that appear in eq 4 are

$$\left.\begin{aligned}(\partial x_i/\partial n_j) &= -x_i x_j/n_j \quad (j \neq i)\\ &= (1 - x_i)x_i/n_i \quad (j = i)\end{aligned}\right\} \tag{5}$$

and

$$\left.\begin{aligned}(\partial n_j/\partial A_j) &= f_j\\ (\partial n_j/\partial f_j) &= A_j\end{aligned}\right\} \tag{6}$$

the overall standard uncertainty of x_i is

$$u^2(x_i) = (\partial x_i/\partial T)^2 u^2(T) + (\partial x_i/\partial p)^2 u^2(p) + [x_i(1 - x_i)]^2[u_r^2(f_i) + u_r^2(A_i)] + \sum_{j\neq i}(x_i x_j)^2[u_r^2(f_j) + u_r^2(A_j)] \tag{7}$$

where $u_r(X)$ is the standard relative uncertainty of variable X. The standard relative uncertainties of the response factors are given by

$$u_r^2(f_j) = [u_r^2(n_j) + u_r^2(A_j)]_{cal} \tag{8}$$

where subscript "cal" denotes the calibration measurement for component j. The relative standard uncertainty $u_r(n_j)$ of the calculated amount of each pure component in the calibration measurement is further related to the uncertainties of the pressure, temperature, and the EoS. The standard uncertainties of these quantities as detailed above lead to combined standard uncertainties varying between $1{\cdot}10^{-6}$ and $3.5{\cdot}10^{-3}$ depending on the component and state point.

2.6. Validation. To validate the apparatus, VLE measurements were made previously on (CO_2 + $C_{10}H_{22}$)[12] and found to be in good agreement with the literature. As a further validation, we have measured VLE data for (C_7H_{14} + CO_2) and compared the results with the extensive literature data.

The first experimental study on the system (C_7H_{16} + CO_2) was that of Kalra et al.[47] who reported VLE composition at temperatures T = (310.65, 352.59, 394.26 and 477.21) K and at several pressures between the vapor pressures of C_7H_{16} and the critical point of the system. Inomata et al.[48] studied the VLE at temperatures from (394 to 502) K and pressures up to p = 12.84 MPa using a flow-type apparatus designed to limit the effects of thermal decomposition at high temperatures. In the study of Sako et al.,[49] VLE data for this system were measured at T = 343 K. King and Al-Najjar[50] measured the solubility of carbon dioxide as a function of temperature in C_7H_{16} and other alkanes at p = 0.1 MPa and reported that the solubilities of carbon dioxide, hydrogen sulfide, and propane increased with increasing alkane chain length. Choi and Yeo[51] presented composition and critical-point data of the binary mixture measured in a variable-volume view cell. Dew points and bubble points were also obtained by visual observation. Fenghour et al.[52] reported phase behavior and density of the binary mixture at temperatures T = (301.76, 321.08 and 362.90) K. The measurements were carried out in an automated isochoric instrument with a claimed relative uncertainty of better than 0.1 %. In the study of Mutelet et al.,[53] phase equilibria and bubble-point pressures of the binary mixture were measured on 12 isotherms at temperatures from (310.65 to 413.15) K using the synthetic method. A 12.4 cm^3 equilibrium cell with a window in sapphire was used. The phase transitions resulting from pressure variation were observed by

DOI: 10.1021/acs.jced.5b00618
J. Chem. Eng. Data 2015, 60, 3670−3681

Table 4. Experimental VLE Data for [C_7H_{16} (1) + CO_2 (2)] at Temperatures T and Pressures p[a]

	phase I (C_7H_{16}-rich)			phase II (CO_2-rich)			phase I	phase II
p/MPa	x_1^{exp}	x_2^{exp}	$u(x_2)$	x_1^{exp}	x_2^{exp}	$u(x_2)$	x_1^{pred}	x_1^{pred}
				T = 352.9 K				
1.89	0.8660	0.1340	0.0023	0.03711	0.96289	0.00115	0.8430	0.03461
3.17	0.7774	0.2226	0.0034	0.02602	0.97398	0.00082	0.7470	0.0236
4.58	0.6669	0.3331	0.0044	0.02122	0.97878	0.00068	0.6539	0.0192
6.64	0.5155	0.4845	0.0049	0.01903	0.98097	0.00061	0.5335	0.0170
8.67	0.3680	0.6320	0.0047	0.02269	0.97731	0.00072	0.4174	0.0170
10.69	0.2226	0.7774	0.0034	0.0414	0.95860	0.00127	0.3106	0.0187
11.63	0.1066	0.8934	0.0018					
				T = 394.15 K				
2.21	0.8852	0.1148	0.0020	0.10231	0.8977	0.0030	0.8752	0.1027
6.67	0.6232	0.3768	0.0047	0.06449	0.9355	0.0020	0.6480	0.0507
8.03	0.5477	0.4523	0.0049	0.06352	0.9365	0.0018	0.5914	0.0481
9.52	0.4757	0.5243	0.0049	0.06701	0.9330	0.0020	0.5299	0.0470
11.54	0.3601	0.6399	0.0047	0.08340	0.9166	0.0024	0.4524	0.0480
13.41	0.2416	0.7584	0.0037	0.1241	0.8759	0.0034	0.3819	0.0514
13.95	0.1782	0.8218	0.0030					

[a]Notation: x_i denotes the mole fraction of component i, $u(x_i)$ denotes standard uncertainty of x_i, and $u(x_1) = u(x_2)$, together with SAFT-VR predictions. Standard uncertainties are $u(T)$ = 0.05 K and $u(p)$ = 0.005 MPa.

visualization through the sapphire window. Recently, Lay et al.[54] studied the bubble point pressures and the phase behavior of the binary mixture at different CO_2 mole fractions ranging from 0.502 to 0.91 and at temperatures in the range from 293.15 to 313.15 K.

Our validation measurements were made on (C_7H_{16} + CO_2) at T = 352.9 K and T = 394.15 K, at pressures up to 14 MPa, and the results, presented in Table 4, are compared with the literature data in Figure 3. Good agreement can be observed between our measurements and those data reported at T = 394.0 K;[48] T = 394.26 K;[47] T = 352.59 K;[47] T = 352.59 K;[53] and T = 394.13 K.[53]

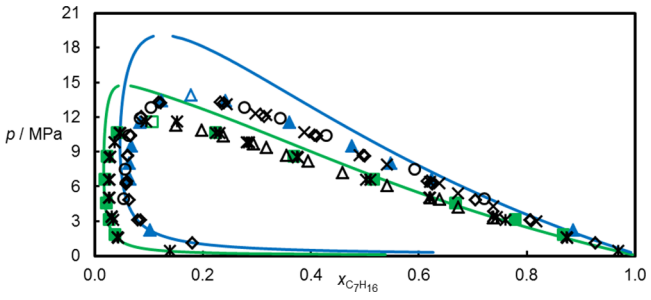

Figure 3. Isothermal pressure composition (p, x) phase diagram for the (C_7H_{16} + CO_2) system at T = 352.9 K (green) and T = 394.15 K (blue). Filled symbol correspond to coexisting-phase data measured in this work, open colored symbols denote UCEP, and continuous curves correspond to SAFT-VR. Open black symbols correspond to published data for the binary system (C_7H_{16} + CO_2): ○, T = 394.01 K;[48] ◊, T = 394.26 K;[47] ∗, T = 352.59 K;[47] △, T = 352.59 K;[53] and ×, T = 394.13 K.[53]

3. EXPERIMENTAL RESULTS

The binary system (C_7H_{16} + CO_2) exhibits types II phase behavior while the binary systems of (CO_2 + H_2O) and (C_7H_{16} + H_2O) exhibit types III phase behavior, according to the classification of Van Konynenburg and Scott.[55,56] As a consequence, mixtures of this type possess a liquid−liquid equilibrium (LLE) immiscibility region and hence, a VLLE region is expected. The characteristic VLLE equilibrium curves of binary systems appear as regions in ternary systems, which can extend to wide ranges of pressures and temperatures depending on the mixture. For (C_7H_{16} + CO_2 + H_2O), this region occurs over a wide range of conditions because of the differences in volatility and size between the CO_2 and the C_7H_{16} molecules. The region within which the three fluid phases coexist is bounded at high pressures by the UCEP locus, above which there is only a single nonaqueous phase in coexistence with the water-rich liquid.

The compositions of the three coexisting fluid phases have been determined along five isotherms at temperatures of (323.15, 343.15, 363.15, 388.15 and 413.15) K and at pressures up to the UCEP. The experimental VLLE data are given in Table 5 together with the estimated standard uncertainties and predictions from SAFT-VR, while the UCEP data are given in Table 6.

The overall standard uncertainties of the experimental phase compositions may be exemplified by the results at the median temperature and pressure as follows (components are designated as 1 = C_7H_{16}, 2 = CO_2, and 3 = H_2O). In the heptane-rich phase, where $x_1 \approx 0.53$, $x_2 \approx 0.45$ and $x_3 \approx 0.02$, we have $u(x_1) \approx u(x_2) \approx 0.0035$ and $u(x_3) = 0.0005$. In the carbon dioxide-rich phase, where $x_1 \approx 0.03$, $x_2 \approx 0.96$, and $x_3 \approx 0.01$, we have $u(x_1) \approx u(x_2) \approx 0.001$ and $u(x_3) = 0.0003$. Finally, in the water-rich phase where $x_1 \approx 5{\cdot}10^{-5}$, $x_2 \approx 0.01$ and $x_3 \approx 0.99$, we have $u(x_1) \approx 4{\cdot}10^{-6}$, $u(x_2) \approx 0.0003$, and $u(x_3) = 0.003$.

4. MODELING

In this work, we employed SAFT-VR to predict the phase behavior of the mixture, and kept the models as consistent as possible with previous work.[12,13] Within SAFT-VR, molecules are modeled as chains of tangent hard spheres that interact through a square-well intermolecular potential. Association by means of directional interactions such as hydrogen bonds is mediated through association sites. A standard four-association-site model is used for water, with two sites of each type. The model parameters for each pure component are collected in Table 7. These were presented in previous works[57−60] and

DOI: 10.1021/acs.jced.5b00618
J. Chem. Eng. Data 2015, 60, 3670−3681

Table 5. Experimental VLLE Data for [C_7H_{16} (1) + CO_2 (2) + H_2O (3)] at Temperatures T and Pressures p[a]

phase	p/MPa	x_1^{exp}	$u(x_1)$	x_2^{exp}	$u(x_2)$	x_3^{exp}	$u(x_3)$	x_1^{pre}	x_2^{pre}	x_3^{pre}
					T = 323.15 K					
I	2.04	0.8159	0.0030	0.1797	0.0030	0.00440	0.00017	0.7676	0.2306	0.0018
II	2.04	0.0153	0.0030	0.9783	0.0030	0.00640	0.00020	0.0109	0.9820	0.0071
III	2.04	0.000191	0.000008	0.00651	0.00021	0.99330	0.00021	$1.00\cdot10^{-08}$	0.0056	0.9944
I	3.31	0.6947	0.0042	0.3005	0.0042	0.00480	0.00018	0.6450	0.3530	0.0020
II	3.31	0.0127	0.0025	0.9818	0.0025	0.00550	0.00017	0.0078	0.9873	0.0049
III	3.31	0.000137	0.000008	0.01012	0.00033	0.98974	0.00033	$3.69\cdot10^{-14}$	0.0088	0.9912
I	4.40	0.5890	0.0048	0.40519	0.00481	0.00581	0.00020	0.5481	0.4496	0.0022
II	4.40	0.0101	0.0021	0.9866	0.0021	0.00330	0.00010	0.0068	0.9891	0.0041
III	4.40	0.000232	0.000010	0.01278	0.00041	0.98699	0.00041	$3.71\cdot10^{-14}$	0.0114	0.9886
I	5.57	0.4679	0.0049	0.5255	0.0049	0.00660	0.00023	0.4484	0.5490	0.0026
II	5.57	0.0094	0.0017	0.9887	0.0017	0.00190	0.00006	0.0063	0.9901	0.0036
III	5.57	0.000220	0.000008	0.01572	0.00049	0.98406	0.00049	$3.65\cdot10^{-14}$	0.0140	0.9860
I	6.94	0.3093	0.0044	0.6830	0.0044	0.00770	0.00025	0.3307	0.6660	0.0033
II	6.94	0.01001	0.00129	0.98781	0.00129	0.00218	0.00007	0.0061	0.9904	0.0034
III	6.94	0.000121	0.000006	0.01769	0.00055	0.98219	0.00055	$3.44\cdot10^{-14}$	0.0167	0.9833
					T = 343.15 K					
I	2.05	0.8426	0.0027	0.1492	0.0025	0.00820	0.00030	0.8132	0.1832	0.0037
II	2.05	0.0273	0.0031	0.9593	0.0031	0.01340	0.00042	0.0233	0.9594	0.0173
III	2.05	0.000058	0.000007	0.00522	0.00017	0.99472	0.00017	$2.54\cdot10^{-13}$	0.0045	0.9955
I	4.11	0.6822	0.0044	0.3086	0.0042	0.00920	0.00031	0.6544	0.3414	0.0041
II	4.11	0.0179	0.0023	0.9733	0.0023	0.00880	0.00027	0.0147	0.9752	0.0102
III	4.11	0.000102	0.000007	0.00961	0.00031	0.99029	0.00031	$2.65\cdot10^{-13}$	0.0089	0.9911
I	6.00	0.5356	0.0049	0.4544	0.0049	0.01000	0.00033	0.5262	0.4690	0.0047
II	6.00	0.0171	0.0016	0.9765	0.0017	0.00640	0.00020	0.0127	0.9791	0.0082
III	6.00	0.000122	0.000007	0.01311	0.00041	0.98677	0.00041	$2.67\cdot10^{-13}$	0.0124	0.9876
I	8.00	0.3727	0.0048	0.6159	0.0048	0.01140	0.00037	0.3999	0.5944	0.0057
II	8.00	0.02141	0.00115	0.97391	0.00115	0.00468	0.00014	0.0126	0.9800	0.0074
III	8.00	0.000079	0.000004	0.01633	0.00051	0.98359	0.00051	$2.61\cdot10^{-13}$	0.0157	0.9843
I	10.00	0.2012	0.0035	0.7862	0.0035	0.01260	0.00041	0.2729	0.7197	0.0075
II	10.00	0.03089	0.00115	0.96404	0.00115	0.00507	0.00016	0.0138	0.9788	0.0074
III	10.00	0.000043	0.000003	0.01842	0.00058	0.98154	0.00057	$2.41\cdot10^{-13}$	0.0185	0.9815
					T = 363.15 K					
I	1.85	0.8443	0.0031	0.1271	0.0028	0.02856	0.00092	0.8601	0.1329	0.0070
II	1.85	0.0536	0.0033	0.9117	0.0035	0.03470	0.00105	0.0490	0.9093	0.0417
III	1.85	0.000047	0.000007	0.003503	0.000129	0.99645	0.00011	$1.54\cdot10^{-12}$	0.0034	0.9966
I	3.16	0.7786	0.0042	0.2003	0.0045	0.02110	0.00066	0.7700	0.2227	0.0074
II	3.16	0.0371	0.0027	0.9376	0.0028	0.02530	0.00078	0.0327	0.9406	0.0267
III	3.16	0.000062	0.000007	0.00691	0.00023	0.99303	0.00023	$1.59\cdot10^{-12}$	0.0059	0.9941
I	4.93	0.6612	0.0044	0.3168	0.0044	0.02199	0.00068	0.6606	0.3315	0.0079
II	4.93	0.0295	0.0020	0.9527	0.0021	0.01780	0.00055	0.0253	0.9553	0.0194
III	4.93	0.0000063	0.000007	0.01042	0.00034	0.98957	0.00033	$1.65\cdot10^{-12}$	0.0090	0.9910
I	7.00	0.5275	0.0049	0.4488	0.0049	0.02377	0.00072	0.5459	0.4453	0.0088
II	7.00	0.0265	0.00141	0.9603	0.0016	0.01320	0.00041	0.0226	0.9615	0.0159
III	7.00	0.000049	0.000006	0.01289	0.00041	0.98706	0.00041	$1.68\cdot10^{-12}$	0.0123	0.9877
I	9.00	0.3984	0.0049	0.5778	0.0049	0.02380	0.00072	0.4437	0.5464	0.0100
II	9.00	0.0292	0.00113	0.9598	0.0013	0.01100	0.00034	0.0225	0.9630	0.0146
III	9.00	0.000046	0.000004	0.01430	0.00045	0.98565	0.00045	$1.67\cdot10^{-12}$	0.0152	0.9848
I	11.00	0.2599	0.0041	0.7152	0.0042	0.02490	0.00076	0.3454	0.6430	0.0117
II	11.00	0.0432	0.0014	0.9465	0.0016	0.01030	0.00033	0.0243	0.9615	0.0142
III	11.00	0.000037	0.000003	0.01571	0.00049	0.98425	0.00049	$1.62\cdot10^{-12}$	0.0177	0.9823
					T = 388.15 K					
I	2.16	0.8654	0.0024	0.1065	0.0020	0.02810	0.00089	0.8678	0.1175	0.0147
II	2.16	0.0920	0.0034	0.8077	0.0045	0.10030	0.00280	0.0883	0.8257	0.0860
III	2.16	0.000079	0.000007	0.00300	0.00013	0.99692	0.00011	$1.26\cdot10^{-11}$	0.0032	0.9968
I	5.00	0.7026	0.0041	0.2690	0.0040	0.02840	0.00088	0.7113	0.2728	0.0158
II	5.00	0.0561	0.0023	0.9037	0.0027	0.04020	0.00120	0.0495	0.9066	0.0439
III	5.00	0.000108	0.000008	0.00831	0.00028	0.99158	0.00027	$1.35\cdot10^{-11}$	0.0078	0.9922
I	7.50	0.5627	0.0049	0.4037	0.0048	0.03360	0.00100	0.5921	0.3907	0.0172
II	7.50	0.0489	0.0016	0.9219	0.0018	0.02920	0.00089	0.0421	0.9237	0.0342
III	7.50	0.000119	0.000007	0.01181	0.00038	0.98807	0.00038	$1.40\cdot10^{-11}$	0.0115	0.9885

DOI: 10.1021/acs.jced.5b00618
J. Chem. Eng. Data 2015, 60, 3670−3681

Table 5. continued

phase	p/MPa	x_1^{exp}	$u(x_1)$	x_2^{exp}	$u(x_2)$	x_3^{exp}	$u(x_3)$	x_1^{pre}	x_2^{pre}	x_3^{pre}
					T = 388.15 K					
I	10.00	0.4242	0.0049	0.5385	0.0049	0.03730	0.00110	0.4843	0.4967	0.0191
II	10.00	0.0559	0.0014	0.9200	0.0017	0.02410	0.00074	0.0411	0.9287	0.0302
III	10.00	0.000149	0.000006	0.01289	0.00041	0.98696	0.00041	$1.43\cdot10^{-11}$	0.0148	0.9852
I	12.10	0.2997	0.0045	0.6595	0.0047	0.04080	0.00122	0.4024	0.5766	0.0210
II	12.10	0.0766	0.0021	0.9018	0.0023	0.02160	0.00066	0.0433	0.9277	0.0290
III	12.10	0.000073	0.000003	0.01452	0.00047	0.98541	0.00045	$1.43\cdot10^{-11}$	0.0172	0.9828
					T = 413.15 K					
I	1.87	0.8961	0.0023	0.0611	0.0014	0.04280	0.00132	0.9044	0.0675	0.0280
II	1.87	0.1847	0.0042	0.6479	0.0057	0.16740	0.00426	0.1841	0.6121	0.2038
III	1.87	0.000128	0.000008	0.00168	0.00013	0.99819	0.00010	$8.64\cdot10^{-11}$	0.0020	0.9980
I	5.00	0.7291	0.0040	0.2233	0.0035	0.04760	0.00141	0.7486	0.2218	0.0296
II	5.00	0.0926	0.0025	0.8280	0.0035	0.07940	0.00226	0.0891	0.8214	0.0895
III	5.00	0.000112	0.000008	0.00603	0.00021	0.99386	0.00020	$9.36\cdot10^{-11}$	0.0068	0.9932
I	8.00	0.5685	0.0049	0.3672	0.0047	0.06430	0.00184	0.6197	0.3486	0.0317
II	8.00	0.0841	0.0018	0.8588	0.0027	0.05710	0.00167	0.0720	0.8625	0.0655
III	8.00	0.000129	0.000007	0.00950	0.00033	0.99037	0.00031	$9.93\cdot10^{-11}$	0.0110	0.9890
I	11.00	0.4139	0.0049	0.5096	0.0049	0.07650	0.00214	0.5037	0.4616	0.0347
II	11.00	0.1174	0.0024	0.8368	0.0030	0.04580	0.00136	0.0691	0.8746	0.0563
III	11.00	0.000143	0.000006	0.01242	0.00041	0.98744	0.00040	$1.03\cdot10^{-10}$	0.0148	0.9852
I	13.00	0.2814	0.0044	0.6340	0.0048	0.08460	0.00236	0.4306	0.5322	0.0372
II	13.00	0.1688	0.0033	0.7910	0.0037	0.04020	0.00119	0.0716	0.8748	0.0535
III	13.00	0.000207	0.000007	0.01411	0.00045	0.98568	0.00045	$1.05\cdot10^{-10}$	0.0172	0.9828

[a]Notation: x_i denotes the mole fraction of component i and $u(x_i)$ denotes standard uncertainty of x_i, together with SAFT-VR predictions. Standard uncertainties are $u(T)$ = 0.05 K and $u(p)$ = 0.005 MPa. Phases I, II, and III are heptane-, CO_2-, and water-rich, respectively.

Table 6. Experimental LLE Data for [C_7H_{16} (1) + CO_2 (2) + H_2O (3)] at the Upper Critical End Point at Temperatures T and Pressures p[a]

		phase II						phase III					
T/K	p/MPa	x_1^{exp}	$u(x_1)$	x_2^{exp}	$u(x_2)$	x_3^{exp}	$u(x_3)$	x_1^{exp}	$u(x_1)$	x_2^{exp}	$u(x_2)$	x_3^{exp}	$u(x_3)$
323.15	9.06	0.04148	0.00091	0.95581	0.00091	0.00271	0.000051	0.000080	0.000004	0.02011	0.00039	0.97981	0.00039
343.15	10.82	0.09938	0.00081	0.89460	0.00081	0.00602	0.00011	0.000110	0.000002	0.01879	0.00041	0.98110	0.00040
363.15	12.20	0.1338	0.0011	0.8550	0.0010	0.01118	0.00023	0.000090	0.000002	0.01662	0.00035	0.98329	0.00035
388.15	13.21	0.1622	0.0016	0.8164	0.0015	0.02142	0.00047	0.000030	0.000002	0.01578	0.00033	0.98419	0.00032
413.15	13.33	0.2220	0.0026	0.7391	0.0023	0.03891	0.00084	0.000270	0.000005	0.01471	0.00032	0.98502	0.00032

[a]Notation: x_i denotes the mole fraction of component i and $u(x_i)$ denotes standard uncertainty of x_i. Standard uncertainties are $u(T)$ = 0.05 K and $u(p)$ = 0.005 MPa. Phases II and III are nonaqueous and aqueous, respectively.

Table 7. SAFT-VR Parameters Used in This Work[a]

cmpd	ref	m	σ_{ii}/nm	(ε_{ii}/k_B)/K	λ_i	$(\varepsilon_{ii}^{HB}/k_B)$/K	$r_{c,ii}$/nm
H_2O	57	1.0	0.30342	250.00	1.7889	1400.0	0.210822
CO_2	58,59	2.0	0.27864	179.27	1.5157		
C_7H_{16}	60	3.0	0.15574	253.28	3.9567		

[a]Notation: m_i is the number of square-well segments in a molecule, σ_{ii} is the hard-core diameter, λ_{ii} and ε_{ii} are the range and the depth of the square-well potential, and ε_{ii}^{HB} and $r_{c,ii}$ are those of the hydrogen-bonding interaction.

obtained from fits to vapor pressure and saturated liquid density data.

In the application of the models to binary mixtures, only the unlike energies have been modified by means of binary interaction parameters. These are temperature-independent, and therefore a single binary interaction parameter is used per pair of compounds. The binary interaction parameter for the system (C_7H_{16} + CO_2) was predicted using a modification of the Hudson and McCoubrey combining rules for square-well intermolecular potentials.[23] This assumes that an estimation for the unlike interaction energy can be obtained by equating the expression for the attractive part of the intermolecular potential to the sum of all possible attractive interaction energies between the corresponding pair of molecules (i.e., London dispersion, Keesom, Debye, and quadrupole interactions, among others). For this mixture, where there are no dipole−dipole and no hydrogen-bonding interactions, the modification of Hudson and McCoubrey combining rules can be shown to lead to the following expression for the k_{ij} unlike interaction:

DOI: 10.1021/acs.jced.5b00618
J. Chem. Eng. Data 2015, 60, 3670−3681

$$k_{ij} = 1 - \left[\frac{3}{m_i m_j \sigma_{ij}^3 (\lambda_{ij}^3 - 1)} \left(\frac{1}{2\sigma_{ij}^3 (4\pi\varepsilon_r\varepsilon_0)^2} \frac{I_i I_j}{(I_i + I_j)} \alpha_{0,i}^* \alpha_{0,j}^* + \frac{1}{5\sigma_{ij}^5 (4\pi\varepsilon_r\varepsilon_0)^2} \frac{3}{2} (Q_i^2 \alpha_{0,j}^* + Q_j^2 \alpha_{0,i}^*) \right) \frac{1}{\sqrt{(\varepsilon_{ii}\varepsilon_{jj})}} \right] \quad (9)$$

where ε_0 is the permittivity of vacuum, ε_r is the relative permittivity (or dielectric constant) of the medium, and I_i, Q_i, and $\alpha_{0,i}^*$ are the ionization energy, quadrupole moment, and electronic polarizability of molecule i, respectively.

In this calculation, the dependence of the relative permittivity on temperature and density is neglected by making the approximation that $\varepsilon_r = 1$ in the nonaqueous phases.[61] The other parameters are taken to be $Q_1 = 0$, $Q_2 = -1.4 \cdot 10^{-39}$ C·m^2, $I_1 = 1.6 \cdot 10^{-18}$ J, and $I_2 = 2.2 \cdot 10^{-18}$ J, where 1 = C_7H_{16} and 2 = CO_2, respectively.[62] The binary interaction parameter for (C_7H_{16} + CO_2) determined from eq 9 is $k_{12} = 0.1162$.

Differences between the relative permittivity of each coexisting liquid phase in aqueous systems are not negligible due to the high value of the relative permittivity of water (in comparison to that of the other phases). According to the modified Hudson and McCoubrey combining rules for polar molecules presented as eq 9, these differences lead to the prediction of different binary interaction parameters for each liquid phase in aqueous mixtures. For the sake of simplicity, here we opt for a single k_{ij} value, instead, for each aqueous pair (C_7H_{16} + H_2O) and (CO_2 + H_2O). The binary interaction parameter for (C_7H_{16} + H_2O) has been kept to the value of k_{13} = 0.2725 that was optimized to fit VLE and saturated decane-rich phase LLE data for ($C_{10}H_{22}$ + H_2O).[12] This leads to good agreement with the available experimental data for the (C_7H_{16} + H_2O) system, but the composition of the aqueous phase is under predicted, as it was with the ($C_{10}H_{22}$ + H_2O) mixture.[12] A binary interaction parameter value of $k_{23} = -0.06$ is used for the (CO_2 + H_2O) system, optimized in previous work.

5. DISCUSSION AND COMPARISON WITH EXPERIMENT

In Figure 3, we compare the VLE data with SAFT-VR for the binary system (C_7H_{16} + CO_2). It can be seen that the SAFT-VR prediction is good at low pressures. At high pressures approaching the critical region, the equation over predicts the pressure for given compositions at these temperatures. This is a known difficulty of classical equations of state, which are based in a mean-field approximation and therefore neglect the density and composition fluctuations that become important in the critical region.

Figure 4 shows the UCEP curve for the ternary system (CO_2 + C_7H_{16} + H_2O). A comparison with the experimental critical points[47,51] for the binary system (CO_2 + C_7H_{16}) is shown, so that the effect of adding a third component (H_2O) on the critical curve of the system can be analyzed. It can be observed that the presence of water has no significant effect on the UCEP curve, reflecting the very small amounts of H_2O present in the nonaqueous phases.

The experimental results are also plotted in the form of isothermal triangular diagrams in Figure 5. It can be seen that the three-phase region for a given pressure diminishes as the critical point between the CO_2- and C_7H_{16}-rich phases is approached. Comparing the subfigures, it can also be observed that the three-phase region diminishes as temperature increases. In general, quite good agreement between experimental data and theory is observed; it is worth noting the good performance of the equation in predicting the phase behavior at different temperatures even with temperature-independent binary interaction parameters.

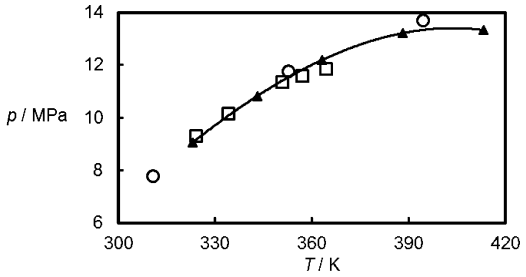

Figure 4. A plot showing the UCEP pressures as a function of temperatures ▲, this work for the ternary mixture (C_7H_{16} + CO_2 + H_2O); ○, ref 47 and □, ref 51 critical data for the binary mixture (C_7H_{16} + CO_2); solid line represents a polynomial fit to our data.

In Figure 6, we compare the experimental VLLE data with the predictions of the SAFT-VR model by means of isothermal (p, x_i) diagrams for the three coexisting phases. The CO_2 and H_2O mole fractions in the aqueous phase are shown in Figure 6a,b while, in Figure 6c,d, we show the CO_2 and H_2O mole fractions in the hydrocarbon-rich phase. The mole fraction of CO_2 in the hydrocarbon-rich phase shows a similar dependence upon temperature and pressure as found in the aqueous phase. The mole fraction of CO_2 in the hydrocarbon-rich phase agrees well with predictions from SAFT-VR, but the H_2O content is substantially under predicted by SAFT-VR. The mole fractions of C_7H_{16} and H_2O in the CO_2-rich phase are plotted in Figure 6e,f. The experimental H_2O mole fractions are generally in fair agreement with the SAFT-VR predictions. As commented in Figure 3, SAFT-VR agrees reasonably well with the mole fraction of C_7H_{16} at low pressures but strongly underpredicts the mole fraction of C_7H_{16} in the proximity of the UCEP.

In the following section, the corresponding binary systems have been compared with the VLLE experimental data of the ternary mixture. We use such a comparison to draw conclusions regarding the effect of adding one component on the phase behavior of the other two.

Influence of H_2O on the Phase Behavior of (C_7H_{16} + CO_2). The amount of H_2O present in the C_7H_{16}-rich and CO_2-rich gas phases is generally small and should have a small effect on the mutual solubility between C_7H_{16} and CO_2 as shown in Figure 7. The H_2O content of the C_7H_{16}-rich and CO_2-rich phases increases with temperature. In the CO_2-rich phase it rapidly decreases as pressure increases. However, in the C_7H_{16}-rich phase, it slightly increases as pressure increases. In this figure, the total pressure is plotted as a function of the mole fractions of C_7H_{16} in the C_7H_{16}-rich liquid phase and the CO_2-rich gas phase at temperatures of (323.15, 363.15 and 413.15) K. These experimental data are compared with the binary system (C_7H_{16} + CO_2) data published by Mutelet et al.[53] at T = (323.20, 363.15 and 413.15) K and He[63] et al. at T = 323.15. It can be seen that, as temperature increases, the saturated region shifts toward lower concentrations of C_7H_{16} and becomes larger in size. It can also be seen that the effect of the presence of H_2O is small in both the low- and high-pressure regions. Comparisons between the SAFT-VR calculations for the

DOI: 10.1021/acs.jced.5b00618
J. Chem. Eng. Data 2015, 60, 3670−3681

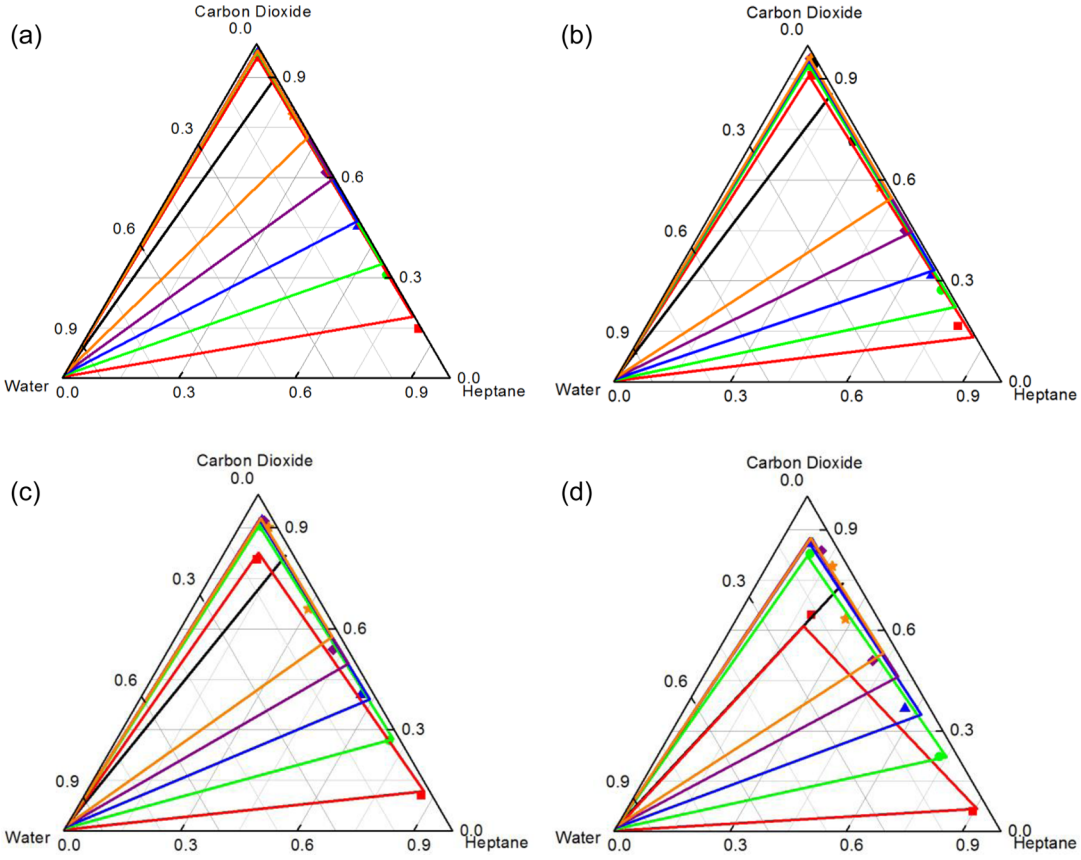

Figure 5. Isothermal composition diagram for the (C_7H_{16} + CO_2 + H_2O) system at (a) T = 343.15 K, (b) T = 363.15 K, (c) T = 388.15 K and (d) T = 413.15 K. The symbols correspond to VLLE data measured in this work at the following average pressures: ■, p = 2.10 MPa; ●, p = 4.50 MPa; ▲, p = 7.20 MPa; ◆, p = 9.50 MPa ; ⬟, p = 11.00 MPa; and ★, p = 12.00 MPa. The continuous black line is the measured tie-line between the two coexisting phases remaining after the critical point between the CO_2-rich and the C_7H_{16}-rich phases. The continuous colored lines are SAFT-VR predictions of the three-phase equilibrium region for every pressure data point plotted.

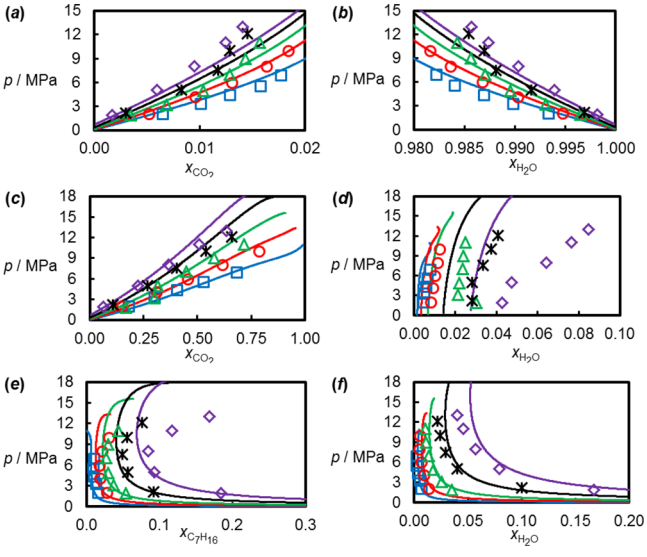

Figure 6. Isothermal pressure−composition (p, x) phase diagram for the (C_7H_{16} + CO_2 + H_2O) system in the H_2O-rich phase (a, b), C_7H_{16}-rich phase (c, d), and CO_2-rich gas phase (e, f) under VLLE conditions. Symbols correspond to the data gathered in this work at □, T = 323.15 K; ○, T = 343.15 K; △, T = 363.15 K; ∗, T = 388.15 K; and ◊, T = 413.15 K. The continuous curves are SAFT-VR predictions of the three phases equilibrium region at the corresponding temperatures. (indicated by colors).

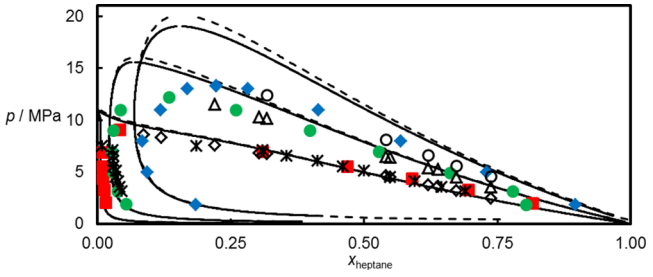

Figure 7. Isothermal pressure−composition phase diagram for the (C_7H_{16} + CO_2 + H_2O) system at T = 323.15 K (red), T = 363.15 K (green), and T = 413.15 K (blue). Filled symbols correspond to the coexisting-phase data measured in this work, continuous curves correspond to SAFT-VR predictions for the ternary mixture, and discontinuous curves correspond to the SAFT-VR predictions for the binary system (C_7H_{16} + CO_2). Open black symbols correspond to published data for the binary system (C_7H_{16} + CO_2): ◊, T = 323.20;[53] △, T = 363.15;[53] ∗ T = 323.15;[63] ○, T = 413.15.[53]

ternary and the binary system lead to the same conclusion. It can be observed that the theory agrees with experiment well at low pressures but deviates in the critical region, as noted earlier.

Influence of C_7H_{16} on the Phase Behavior of (CO_2 + H_2O). The effects of C_7H_{16} on the miscibility of CO_2 and H_2O can be illuminated by comparison with the binary (CO_2 + H_2O) system and, for this purpose, we consider the models of Duan et al.[64] and Spycher et al.[65,66] and define K values by K_i =

DOI: 10.1021/acs.jced.5b00618
J. Chem. Eng. Data 2015, 60, 3670−3681

X_i^{II}/X_i^{III}, where X_i^{II} is the mole fraction of component i in the CO_2-rich gas phase and X_i^{III} is the mole fraction of component i in the H_2O-rich liquid phase. Figure 8 compares the present

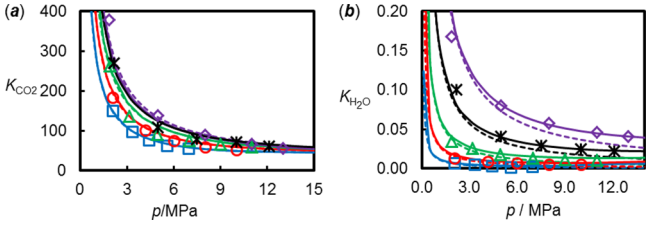

Figure 8. K factor of either CO_2 (a) or H_2O (b) as functions of pressure. Symbols correspond to the data of this work under VLLE conditions at □, T = 323.15 K; ○, T = 343.15 K; △, T = 363.15 K; ∗, T = 388.15 K; and ◊, T = 413.15 K. Dotted and continues curves represent binary data for the system (CO_2 + H_2O) obtained from the model of Duan et al.[64] and Spycher et al.[65,66] at the corresponding temperatures (indicated by the same color).

experimental K values of CO_2 and H_2O for the ternary system under VLLE conditions with those for the (CO_2 + H_2O) binary system as calculated from the models of Duan et al. and Spycher et al. In the case of K_{CO_2}, shown in Figure 8a, the experimental data differ only slightly from the two models but suggest that the solubility of CO_2 in the aqueous phase is slightly increased by the addition of C_7H_{16}. Turning now to K_{H_2O}, the comparison in Figure 8b suggests that the water content of the CO_2-rich phase is slightly reduced by the presence of C_7H_{16}. The model of Duan et al. is less accurate for the CO_2-rich phase as an ideal mixing approximation was applied and is not considered further in this respect.

Influence of CO_2 on the Phase Behavior of (C_7H_{16} + H_2O). The effect of the presence of CO_2 on the phase equilibria of the binary system (C_7H_{16} + H_2O) can be examined by reference to Figure 9. In this figure, we plot the K values of

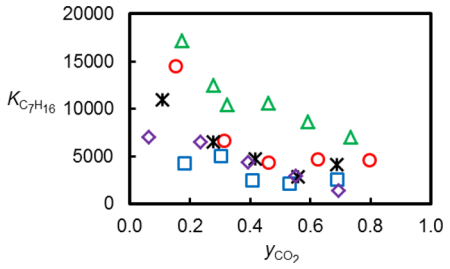

Figure 9. K factor of C_7H_{16} as a function of CO_2 mole fraction. Symbols correspond to the data of this work under VLLE conditions at □, T = 323.15 K; ○, T = 343.15 K; △, T = 363.15 K; ∗, T = 388.15 K; and ◊, T = 413.15 K.

C_7H_{16} determined from the present VLLE data against CO_2 mole fraction in the C_7H_{16}-rich phase. It can be seen that the solubility of C_7H_{16} in the H_2O-rich liquid phase appears to be enhanced by the addition of CO_2. This means that CO_2 acts as a cosolvent. The same observation has been noted previously[11] and so we may conclude that the presence of CO_2 in general increases the solubility of alkanes in H_2O.

6. CONCLUSION

We report a detailed experimental study of vapor−liquid−liquid equilibria for (C_7H_{16} + CO_2 + H_2O) on five isotherms at temperatures from (323.15 to 413.15) K with pressures up to the upper critical end point (UCEP). The results have been compared with the predictions of the statistical associating fluid theory for potentials of variable range (SAFT-VR). In our application of the equation we keep the models used as consistent as possible with previous studies. Only the unlike dispersion energies between each pair of compounds are modified through binary interaction parameters, which are all taken to be temperature-independent. The alkane−H_2O binary interaction parameter is found to be transferable from a previous study with a different alkane, and the alkane−CO_2 one is predicted using a modified Hudson-McCoubrey combining rule. The binary interaction parameter for the carbon dioxide-water interaction is also taken from previous work. A detailed comparison between the SAFT-VR calculations and the experimental data demonstrates the good performance of the theory, applied in predictive mode, for ternary mixtures of alkanes, carbon dioxide, and water.

The behavior of the ternary system was compared with that of the constituent binary subsystems, and it was concluded that adding CO_2 increases the solubility of C_7H_{16} in the H_2O-rich phase. Furthermore, the addition of C_7H_{16} to (CO_2 + H_2O) slightly increases the solubility of CO_2 in the aqueous phase and slightly decreases the H_2O content of the CO_2-rich phase. Finally, the effect of H_2O on the phase behavior of (C_7H_{16} + CO_2) was very small, as expected, given the low amounts of H_2O in the nonaqueous phases.

AUTHOR INFORMATION

Corresponding Author

*E-mail: m.trusler@imperial.ac.uk.

Present Address

§E.F.: Laboratory of Engineering Thermodynamics, University of Kaiserslautern, Erwin-Schrödinger-Straße 44, 67663 Kaiserslautern, Germany.

Funding

This work was carried out as part of the activities of the Qatar Carbonates & Carbon Storage Research Centre (QCCSRC). We gratefully acknowledge the funding of QCCSRC provided jointly by Qatar Petroleum, Shell, and the Qatar Science and Technology Park, and their permission to publish this research.

Notes

The authors declare no competing financial interest.

REFERENCES

(1) Dhima, A.; de Hemptinne, J.-C.; Jose, J. Solubility of Hydrocarbons and CO_2 Mixtures in Water Under High Pressure. *Ind. Eng. Chem. Res.* **1999**, *38*, 3144−3161.

(2) Song, K. Y.; Kobayashi, R. The Water Content of a Carbon Dioxide-Rich Gas Mixture Containing 5.31 mol % Methane Along the Three-Phase and Supercritical Conditions. *J. Chem. Eng. Data* **1990**, *35*, 320−322.

(3) Jarne, C.; Blanco, S. T.; Gallardo, M. A.; Rauzy, E.; Otín, S.; Velasco, I. Dew Points of Ternary Methane (or Ethane) + Carbon Dioxide + Water Mixtures: Measurement and Correlation. *Energy Fuels* **2004**, *18*, 396−404.

(4) Qin, J.; Rosenbauer, R. J.; Duan, Z. Experimental Measurements of Vapor-Liquid Equilibria of the H_2O + CO_2 + CH_4 Ternary System. *J. Chem. Eng. Data* **2008**, *53*, 1246−1249.

(5) Belandria, V.; Eslamimanesh, A.; Mohammadi, A. H.; Théveneau, P.; Legendre, H.; Richon, D. Compositional Analysis and Hydrate Dissociation Conditions Measurements for Carbon Dioxide + Methane + Water System. *Ind. Eng. Chem. Res.* **2011**, *50*, 5783−5794.

DOI: 10.1021/acs.jced.5b00618
J. Chem. Eng. Data 2015, 60, 3670−3681

(6) Beltrán, J. G.; Servio, P. Equilibrium Studies for the System Methane + Carbon Dioxide + Neohexane + Water. *J. Chem. Eng. Data* **2008**, *53*, 1745−1749.
(7) Seo, Y.-T.; Lee, H.; Yoon, J.-H. Hydrate Phase Equilibria of the Carbon Dioxide, Methane, and Water System. *J. Chem. Eng. Data* **2001**, *46*, 381−384.
(8) Ohgaki, K. T.; Sangawa, H.; Matsubara, T.; Nakano, S.; Takano, K. Methane Exploitation by Carbon Dioxide From Gas Hydrates-Phase Equilibria for CO_2−CH_4 Mixed Hydrate System. *J. Chem. Eng. Jpn.* **1996**, *29*, 478−483.
(9) Bruusgaard, H.; Beltrán, J. G.; Servio, P. Solubility Measurements for the CH_4 + CO_2 + H_2O System Under Hydrate−Liquid−Vapor Equilibrium. *Fluid Phase Equilib.* **2010**, *296*, 106−109.
(10) Uchida, T.; Ikeda, I. Y.; Takeya, S.; Kamata, Y.; Ohmura, R.; Nagao, J.; Zatsepina, O. Y.; Buffett, B. A. Kinetics and Stability of CH_4−CO_2 Mixed Gas Hydrates during Formation and Long-Term Storage. *ChemPhysChem* **2005**, *6*, 646−654.
(11) Al Ghafri, S. Z. S.; Forte, E.; Maitland, G. C.; Rodriguez-Henríquez, J. J.; Trusler, J. P. M. Experimental and Modeling Study of the Phase Behavior of (Methane + CO_2 + Water) Mixtures. *J. Phys. Chem. B* **2014**, *118*, 14461−14478.
(12) Forte, E.; Galindo, A.; Trusler, J. P. M. Experimental and Molecular Modeling Study of the Three-Phase Behavior of (n-Decane + Carbon Dioxide + Water) at Reservoir Conditions. *J. Phys. Chem. B* **2011**, *115*, 14591−14609.
(13) Forte, E.; Galindo, A.; Trusler, J. P. M. Experimental and Molecular Modelling Study of the Three-Phase Behaviour of (Propane + Carbon Dioxide + Water) at Reservoir Conditions. *J. Supercrit. Fluids* **2013**, *75*, 30−42.
(14) Galindo, A.; Davies, L. A.; Gil-Villegas, A.; Jackson, G. The Thermodynamics of Mixtures and the Corresponding Mixing Rules in the SAFT-VR Approach for Potentials of Variable Range. *Mol. Phys.* **1998**, *93*, 241−252.
(15) Gil-Villegas, A.; Galindo, A.; Whitehead, P. J.; Mills, S. J.; Jackson, G.; Burgess, A. N. Statistical Associating Fluid Theory for Chain Molecules With Attractive Potentials of Variable Range. *J. Chem. Phys.* **1997**, *106*, 4168−4186.
(16) Brunner, G.; Teich, J.; Dohrn, R. Phase Equilibria in Systems Containing Hydrogen, Carbon Dioxide, Water and Hydrocarbons. *Fluid Phase Equilib.* **1994**, *100*, 253−268.
(17) Chapman, W. G.; Gubbins, K. E.; Jackson, G.; Radosz, M. New Reference Equation of State for Associating Liquids. *Ind. Eng. Chem. Res.* **1990**, *29*, 1709−1721.
(18) Chapman, W. G.; Gubbins, K. E.; Jackson, G.; Radosz, M.; SAFT. Equation-of-State Solution Model for Associating Fluids. *Fluid Phase Equilib.* **1989**, *52*, 31−38.
(19) Wertheim, M. S. Fluids With Highly Directional Attractive Forces. IV. Equilibrium Polymerization. *J. Stat. Phys.* **1986**, *42*, 477−492.
(20) Wertheim, M. S. Fluids With Highly Directional Attractive Forces. III. Multiple Attraction Sites. *J. Stat. Phys.* **1986**, *42*, 459−476.
(21) Wertheim, M. S. Fluids With Highly Directional Attractive Forces. II. Thermodynamic Perturbation Theory and Integral Equations. *J. Stat. Phys.* **1984**, *35*, 35−47.
(22) Wertheim, M. S. Fluids With Highly Directional Attractive Forces. I. Statistical Thermodynamics. *J. Stat. Phys.* **1984**, *35*, 19−34.
(23) Haslam, A. J.; Galindo, A.; Jackson, G. Prediction of Binary Intermolecular Potential Parameters for Use in Modelling Fluid Mixtures. *Fluid Phase Equilib.* **2008**, *266*, 105−128.
(24) Galindo, A.; Whitehead, P. J.; Jackson, G. Predicting the High-Pressure Phase Equilibria of Water + n-Alkanes Using a Simplified SAFT Theory with Transferable Intermolecular Interaction Parameters. *J. Phys. Chem.* **1996**, *100*, 6781−6792.
(25) Kraska, T.; Gubbins, K. E. Phase Equilibria Calculations with a Modified SAFT Equation of State. 2. Binary Mixtures of n-Alkanes, 1-Alkanols, and Water. *Ind. Eng. Chem. Res.* **1996**, *35*, 4738−4746.
(26) Yakoumis, I. V.; Kontogeorgis, G. M.; Voutsas, E. C.; Hendriks, E. M.; Tassios, D. P. Prediction of Phase Equilibria in Binary Aqueous Systems Containing Alkanes, Cycloalkanes, and Alkenes with the Cubic-plus-Association Equation of State. *Ind. Eng. Chem. Res.* **1998**, *37*, 4175−4182.
(27) Patel, B. H.; Paricaud, P.; Galindo, A.; Maitland, G. C. Prediction of the Salting-Out Effect of Strong Electrolytes on Water + Alkane Solutions. *Ind. Eng. Chem. Res.* **2003**, *42*, 3809−3823.
(28) Voutsas, E. C.; Boulougouris, G. C.; Economou, I. G.; Tassios, D. P. Water/Hydrocarbon Phase Equilibria Using the Thermodynamic Perturbation Theory. *Ind. Eng. Chem. Res.* **2000**, *39*, 797−804.
(29) Karakatsani, E. K.; Kontogeorgis, G. M.; Economou, I. G. Evaluation of the Truncated Perturbed Chain-Polar Statistical Associating Fluid Theory for Complex Mixture Fluid Phase Equilibria. *Ind. Eng. Chem. Res.* **2006**, *45*, 6063−6074.
(30) Li, X.-S.; Englezos, P. Vapor−Liquid Equilibrium of Systems Containing Alcohols, Water, Carbon Dioxide and Hydrocarbons Using SAFT. *Fluid Phase Equilib.* **2004**, *224*, 111−118.
(31) Oliveira, M. B.; Coutinho, J. A. P.; Queimada, A. J. Mutual Solubilities of Hydrocarbons and Water With the CPA EoS. *Fluid Phase Equilib.* **2007**, *258*, 58−66.
(32) Vega, L.; Llovell, F.; Blas, F. Capturing the Solubility Minima of n-Alkanes in Water by Soft-SAFT. *J. Phys. Chem. B* **2009**, *113*, 7621−7630.
(33) Aparicio-Martínez, S.; Hall, K. R. Phase Equilibria in Water Containing Binary Systems From Molecular Based Equations of State. *Fluid Phase Equilib.* **2007**, *254*, 112−125.
(34) Nguyen-Huynh, D.; de Hemptinne, J.-C.; Lugo, R.; Passarello, J.-P.; Tobaly, P. Modeling Liquid−Liquid and Liquid−Vapor Equilibria of Binary Systems Containing Water with an Alkane, an Aromatic Hydrocarbon, an Alcohol or a Gas (Methane, Ethane, CO_2 or H_2S), Using Group Contribution Polar Perturbed-Chain Statistical Associating Fluid Theory. *Ind. Eng. Chem. Res.* **2011**, *50*, 7467−7483.
(35) Pereda, S.; Awan, J. A.; Mohammadi, A. H.; Valtz, A.; Coquelet, C.; Brignole, E. A.; Richon, D. Solubility of Hydrocarbons in Water: Experimental Measurements and Modeling Using a Group Contribution With Association Equation of State (GCA-EoS). *Fluid Phase Equilib.* **2009**, *275*, 52−59.
(36) Papaioannou, V.; Adjiman, C. S.; Jackson, G.; Galindo, A. Simultaneous Prediction of Vapour-Liquid and Liquid-Liquid Equilibria (VLE And LLE) of Aqueous Mixtures With The SAFT-Gamma Group Contribution Approach. *Fluid Phase Equilib.* **2011**, *306*, 82−96.
(37) Emborsky, C. P.; Cox, K. R.; Chapman, W. G. Correlation and Prediction of Water Content in Alkanes Using a Molecular Theory. *Ind. Eng. Chem. Res.* **2011**, *50*, 7791−7799.
(38) Valtz, A.; Chapoy, A.; Coquelet, C.; Paricaud, P.; Richon, D. Vapour-Liquid Equilibria in the Carbon Dioxide-Water System, Measurement and Modelling From 278.2 to 318.2 K. *Fluid Phase Equilib.* **2004**, *226*, 333−344.
(39) Kontogeorgis, G. M.; Michelsen, M. L.; Folas, G. K.; Derawi, S.; von Solms, N.; Stenby, E. H. Ten Years with the CPA (Cubic-Plus-Association) Equation of State. Part 2. Cross-Associating and Multicomponent Systems. *Ind. Eng. Chem. Res.* **2006**, *45*, 4869−4878.
(40) Kontogeorgis, G. M.; Folas, G. K.; Muro-Suñé, N.; Roca Leon, F.; Michelsen, M. L. Les Théories d'Association et le Phénomène de la Solvatation: Application aux Industries du Pétrole et du Gaz, et à la Pétrochimie. *Oil Gas Sci. Technol.* **2008**, *63*, 305−319.
(41) Mac Dowell, N.; Llovell, F.; Adjiman, C. S.; Jackson, G.; Galindo, A. Modeling the Fluid Phase Behavior of Carbon Dioxide in Aqueous Solutions of Monoethanolamine Using Transferable Parameters with the SAFT-VR Approach. *Ind. Eng. Chem. Res.* **2010**, *49*, 1883−1899.
(42) dos Ramos, M. C.; Blas, F. J.; Galindo, A. Modelling the Phase Equilibria and Excess Properties of the Water+Carbon Dioxide Binary Mixture. *Fluid Phase Equilib.* **2007**, *261*, 359−365.
(43) dos Ramos, M. C.; Blas, F. J.; Galindo, A. Phase Equilibria, Excess Properties, and Henry's Constants of the Water + Carbon Dioxide Binary Mixture. *J. Phys. Chem. C* **2007**, *111*, 15924−15934.
(44) Span, R.; Wagner, W. A New Equation of State for Carbon Dioxide Covering the Fluid Region from the Triple-Point Temper-

DOI: 10.1021/acs.jced.5b00618
J. Chem. Eng. Data 2015, 60, 3670−3681

ature to 1100 K at Pressures up to 800 MPa. *J. Phys. Chem. Ref. Data* **1996**, *25*, 1509−1596.
(45) Schedemann, A.; Ihmels, E. C.; Gmehling, J. Liquid Densities of THF and Excess Volumes for the Mixture With Water in a Wide Temperature and Pressure Range. *Fluid Phase Equilib.* **2010**, *295*, 201−207.
(46) Ramos-Estrada, M.; Iglesias-Silva, G. A.; Hall, K. R. Experimental Measurements and Prediction of Liquid Densities For n-Alkane Mixtures. *J. Chem. Thermodyn.* **2006**, *38*, 337−347.
(47) Kalra, H.; Kubota, H.; Robinson, D. B.; Ng, H.-J. Equilibrium phase Properties of the Carbon Dioxide-n-Heptane System. *J. Chem. Eng. Data* **1978**, *23*, 317−321.
(48) Inomata, H.; Arai, K.; Saito, S. Measurement of Vapor-Liquid Equilibria at Elevated Temperatures and Pressures Using a Flow Type Apparatus. *Fluid Phase Equilib.* **1986**, *29*, 225−232.
(49) Sako, T.; Sugeta, T.; Nakazawa, N.; Otake, K.; Sato, M.; Ishihara, K.; Kato, M. High Pressure Vapor-Liquid and Vapor-Liquid-Liquid Equilibria for Systems Containing Supercritical Carbon Dioxide, Water and Furfural. *Fluid Phase Equilib.* **1995**, *108*, 293−303.
(50) King, M. B.; Al-Najjar, H. The Solubilities of Carbon Dioxide, Hydrogen Sulphide and Propane in Some Normal Alkane Solvents—I: Experimental Determinations in the Range 15−70°C and Comparison With Ideal Solution Values. *Chem. Eng. Sci.* **1977**, *32*, 1241−1246.
(51) Choi, E.-J.; Yeo, S.-D. Critical Properties for Carbon Dioxide + n-Alkane Mixtures Using a Variable-Volume View Cell. *J. Chem. Eng. Data* **1998**, *43*, 714−716.
(52) Fenghour, A.; Trusler, J. P. M.; Wakeham, W. A. Densities and Bubble Points of Binary Mixtures of Carbon Dioxide and n-Heptane and Ternary Mixtures of n-Butane, n-Heptane and n-Hexadecane. *Fluid Phase Equilib.* **2001**, *185*, 349−358.
(53) Mutelet, F.; Vitu, S.; Privat, R.; Jaubert, J.-N. Solubility of CO_2 in Branched Alkanes in Order to Extend The PPR78 Model (Predictive 1978, Peng−Robinson Eos With Temperature-Dependent K_{ij} Calculated Through A Group Contribution Method) To Such Systems. *Fluid Phase Equilib.* **2005**, *238*, 157−168.
(54) Lay, E. N. Measurement and Correlation of Bubble Point Pressure in (CO_2 + C_6H_6), (CO_2 + $CH_3C_6H_5$), (CO_2 + C_6H_{14}), and (CO_2 + C_7H_{16}) at Temperatures from (293.15 to 313.15) K. *J. Chem. Eng. Data* **2010**, *55*, 223−227.
(55) Scott, R. L.; Van Konynenburg, P. H. Critical Lines and Phase Equilibria in Binary Van Der Waals Mixtures. *Philos. Trans. R. Soc., A* **1980**, *298*, 495−540.
(56) Scott, R. L.; van Konynenburg, P. H. Static Properties of Solutions. Van der Waals and Related Models for Hydrocarbon Mixtures. *Discuss. Faraday Soc.* **1970**, *49*, 87−97.
(57) Clark, G. N. I.; Haslam, A. J.; Galindo, A.; Jackson, G. Developing Optimal Wertheim-Like Models of Water for Use in Statistical Associating Fluid Theory (SAFT) and Related Approaches. *Mol. Phys.* **2006**, *104*, 3561−3581.
(58) Blas, F. J.; Galindo, A. Study of the High Pressure Phase Behaviour of CO_2+n-Alkane Mixtures Using the SAFT-VR Approach With Transferable Parameters. *Fluid Phase Equilib.* **2002**, *194−197*, 501−509.
(59) Galindo, A.; Blas, F. J. Theoretical Examination of the Global Fluid Phase Behavior and Critical Phenomena in Carbon Dioxide + n-Alkane Binary Mixtures. *J. Phys. Chem. B* **2002**, *106*, 4503−4515.
(60) Paricaud, P.; Galindo, A.; Jackson, G. Modeling the Cloud Curves and the Solubility of Gases in Amorphous and Semicrystalline Polyethylene with the SAFT-VR Approach and Flory Theory of Crystallization. *Ind. Eng. Chem. Res.* **2004**, *43*, 6871−6889.
(61) Lide, D. R. *CRC Handbook of Chemistry and Physics*, 86th ed.; CRC Press/Taylor and Francis: Boca Raton, FL, 2005.
(62) Buckingham, A. D. Electric Moments of Molecules. In *Physical Chemistry*; Eyring, H., Henderson, D., Jost, W., Eds.; Academic Press: New York/London, 1970; Vol. *4*, Molecular Properties.
(63) He, Y.; Lu, Z.; Hu, M. S. Y. Measuring Phase Equilibria of Carbon Dioxide - n-Heptane System by Stoichiometry. *J. East China Univ. Sci. Technol.* **1994**, *20*, 79.
(64) Duan, Z.; Sun, R.; Zhu, C.; Chou, I. M. An Improved Model for the Calculation of CO_2 Solubility in Aqueous Solutions Containing Na^+, K^+, Ca^{2+}, Mg^{2+}, Cl^-, and SO_4^{2-}. *Mar. Chem.* **2006**, *98*, 131−139.
(65) Spycher, N.; Pruess, K. A Phase-Partitioning Model for CO_2−Brine Mixtures at Elevated Temperatures and Pressures: Application to CO_2-Enhanced Geothermal Systems. *Transp. Porous Media* **2010**, *82*, 173−196.
(66) Spycher, N.; Pruess, K.; Ennis-King, J. CO_2-H_2O Mixtures in the Geological Sequestration Of CO_2. I. Assessment and Calculation of Mutual Solubilities From 12 to 100°C and up to 600 bar. *Geochim. Cosmochim. Acta* **2003**, *67*, 3015−3031.
(67) Gil, L.; Avila, S.; García-Giménez, P.; Blanco, S. T.; Berro, C.; Otin, S.; Velasco, I. Dew Points of Binary Propane or n-butane + Carbon Dioxide, Ternary Propane or n-butane + Carbon Dioxide + Water, and Quaternary Propane or n-butane + Carbon Dioxide + Water + Methanol Mixtures: Measurement and Modeling. *Ind. Eng. Chem. Res.* **2006**, *45*, 3974−3980.

DOI: 10.1021/acs.jced.5b00618
J. Chem. Eng. Data 2015, 60, 3670−3681